LEGIBILITY NOTICE

A major purpose of the Technical Information Center is to provide the broadest dissemination possible of information contained in DOE's Research and Development Reports to business, industry, the academic community, and federal, state and local governments.

Although a small portion of this report is not reproducible, it is being made available to expedite the availability of information on the research discussed herein.

ORNL/FEDC-89/3
Dist. Categories UC-423,424

ORNL/FEDC--89/3

Fusion Energy Division DE90 008087

TSC DISRUPTION SCENARIOS AND CIT VACUUM VESSEL FORCE EVOLUTION

R. O. Sayer
Y-K. M. Peng
D. J. Strickler
Fusion Engineering Design Center
Oak Ridge National Laboratory
S. C. Jardin
Princeton Plasma Physics Laboratory

Date published: January 1990

Prepared for the
Office of Fusion Energy
Budget Activity No. AT 15

Prepared by the
OAK RIDGE NATIONAL LABORATORY
Oak Ridge, Tennessee 37831
operated by
MARTIN MARIETTA ENERGY SYSTEMS, INC.
for the
U.S. DEPARTMENT OF ENERGY
under contract DE-AC05-84OR21400

CONTENTS

ABSTRACT

The Tokamak Simulation Code and the TWIR postprocessor code have been used to develop credible plasma disruption scenarios for the Compact Ignition Tokamak (CIT) in order to predict the evolution of forces on CIT conducting structures and to provide results required for detailed structural design analysis. The extreme values of net radial and vertical vacuum vessel (VV) forces were found to be $F_R = -12.0$ MN/rad and $F_Z = -3.0$ MN/rad, respectively, for the CIT 2.1-m, 11-MA design.

Net VV force evolution was found to be altered significantly by two mechanisms not noted previously. The first, due to poloidal VV currents arising from increased plasma paramagnetism during thermal quench, reduces the magnitude of the extreme F_R by 15–50% and modifies the distribution of forces substantially. The second effect is that slower plasma current decay rates give more severe net vertical VV loads because the current decay occurs when the plasma has moved farther from midplane than is the case for faster decay rates.

1. INTRODUCTION

The Compact Ignition Tokamak (CIT) is being designed to achieve ignition with a dense, highly elongated, high-current plasma. Design of the CIT vacuum vessel (VV) is driven strongly by the disruption-induced forces produced by plasma motion and current decay. It is therefore particularly important to employ a model that predicts the time behavior of disruptive effects as accurately as possible.

Vacuum vessel eddy current analyses usually emphasize detailed two- and three-dimesional (2-D and 3-D) finite-element VV representations rather than the treatment of plasma motion and decay. For example, the plasma column is often approximated by a few exponentially decaying current filaments. The rapid plasma motion during the thermal quench is neglected, and the plasma current decay and interaction with induced VV eddy currents are not treated self-consistently.

In this report we describe the use of the Tokamak Simulation Code[1,2] (TSC) and the TWIR postprocessor code to develop self-consistent, credible, "highly severe" plasma disruption scenarios for CIT in order to predict the evolution of forces on CIT conducting structures and to provide results required by the SPARK code[3] for generation of finite-element models for detailed structural design analysis.

The following sections describe TSC and the treatment of poloidal VV currents arising from toroidal flux changes, the TWIR postprocessor code, TSC models of the torus conducting structures, and disruption scenarios and give results and conclusions.

2. TOKAMAK SIMULATION CODE

TSC[1,2] is a numerical model of a free-boundary axisymmetric tokamak plasma interacting with a set of axisymmetric conductors that obey circuit equations with active feedback amplifiers included. Modified magnetohydrodynamic equations are solved inside a domain that includes a plasma region, a vacuum region, and a specified number of solid conductors or coils. Control coils external to the computational grid are also incorporated. The interaction of the plasma (motion and current decay) with passive conducting structures is treated in a self-consistent manner.

TSC uses an inertial enhancement technique to make the solution of the plasma force balance equation

$$\partial \mathbf{m}/\partial t + \mathbf{F}_v(\mathbf{m}) = \mathbf{J} \times \mathbf{B} - \nabla p \qquad (1)$$

computationally feasible. The mass and viscosity terms on the left side of Eq. (1) are multiplied by enhancement factors chosen to make time integration feasible while keeping the left side of Eq. (1) small compared with the terms on the right side. Selected cases must be repeated with smaller enhancement factors to ensure convergence in these quantities.

TSC yields the time evolution of plasma parameters, poloidal flux, and eddy currents induced in internal conductors and internal control (IC) coils. These quantities are used to compute the force histories for passive conducting elements for various disruption scenarios. These forces arise from toroidal currents due to poloidal flux changes. TSC also solves a circuit equation for the VV poloidal eddy current[4] arising from toroidal flux changes. This poloidal VV equation is discussed in Sect. 3.

In the TSC code the thermal quench is initiated by increasing the plasma thermal conductivity by several orders of magnitude, producing an enhanced plasma resistivity and a subsequent current quench. The thermal quench phase typically lasts for 100–200 μs; during this time, beta drops to nearly zero, the current profile broadens, the plasma moves inward 5–15 cm, and the net radial VV force approaches an extreme value. During the subsequent current decay phase, which lasts from a few milliseconds to tens of milliseconds, the net vertical VV force builds to an extreme value.

The TSC code predictions have been compared extensively with experimental results from the Princeton Beta Experiment,[5] the Tokamak Fusion Test Reactor, and DIII-D. Good agreement has been obtained for both plasma current and profile evolution for both disruptive and nondisruptive discharges.

TSC can be used to study the sensitivity of net VV forces to dI_p/dt and to various initial conditions to determine the disruption scenarios that produce the most severe loads. A postprocessor code, TWJR, has been developed to compute and display the time behavior of currents, plasma motion, extreme forces, and force distributions. Examination of the evolution of these quantities has proved to be quite useful in the evaluation of disruption scenarios and in the selection of candidates for the most severe load cases. Examples are presented in later sections.

For load analysis of 3-D CIT conducting structures, the TSC plasma current history output was converted for SPARK to approximately 200 coils whose currents were programmed to vary with time so as to represent the disrupting plasma. SPARK computations with this detailed plasma driver and with finite-element

representations of the 3-D conducting structures yielded induced eddy currents and loads suitable for input to structural analysis codes.

3. POLOIDAL VV CIRCUIT EQUATION AND FORCES

The axisymmetric TSC code determines toroidal VV eddy currents due to poloidal flux changes resulting from major disruptions. However, one source of induced poloidal VV current can be estimated from the difference between the toroidal field and the vacuum field, integrated over the plasma volume. This "paramagnetic" flux, Φ_{para}, which is caused by changes in plasma paramagnetism during the thermal quench, is used in a simple circuit equation[3] in TSC to determine the poloidal VV current, I_{vvpol}. Corresponding force histories are calculated in the TWIR postprocessor code.

3.1. CIRCUIT EQUATION

Consider the VV as a loop with current I_{vvpol} flowing in the poloidal direction (Fig. 1) as a result of change in toroidal flux throughout the plasma volume. Neglect mutual inductances between the VV and the plasma and between the VV and the surrounding structures. The circuit equation is

$$L_{vv}\, dI_{vvpol}/dt + R_{vv}\, I_{vvpol} = -d\Phi_{para}/dt \quad , \tag{2}$$

where L_{vv} is the VV self-inductance and R_{vv} is the resistance to poloidal current flow. Typically, $R_{vv} = 16\ \mu\Omega$, and $L_{vv} = 0.41\ \mu$H. The poloidal current is obtained by integrating Eq. (2) forward in time.

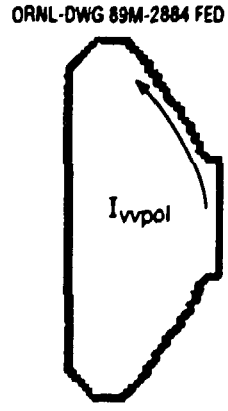

Fig. 1. Poloidal current flow in a tokamak vacuum vessel.

For a major disruption of the type considered here, Φ_{para} increases to a large positive value during the thermal quench. For example, for $dI_p/dt = -3.4$ MA/ms, Φ_{para} increases by 0.78 Wb in about 0.2 ms. Over this time scale, the solution is inductive, and the maximum current is approximately

$$I_{vvpol} \simeq 0.78 \text{ Wb}/0.41\ \mu\text{H} = 1.9 \text{ MA} \quad . \tag{3}$$

The actual maximum current from integration of Eq. (2) is 1.82 MA. As the current quench proceeds, Φ_{para} decreases to zero, and I_{vvpol} decays in a time governed by both the current quench time and the VV L/R time.

3.2. FORCES

The VV is represented as a set of axisymmetric filaments. For the ith filament, let $F_{vvpol}(i)$ be the force, in newtons per radian, on an element of length dl. If $G_0 = XB_t$, where B_t is the vacuum toroidal field, then

$$F_{vvpol}(i) = I_{vvpol} dl G_0/(2\pi X_i) \quad , \tag{4}$$

where X_i is the radius of the ith filament.

Poloidal currents introduce a change in G_0 inside the VV given by $\delta G = I_{vvpol}\ \mu_0/(2\pi)$. For the CIT 2.1-m design, the maximum $\delta G/G$ for the 3.4-MA/ms disruption is 0.017. Therefore, neglect of δG due to poloidal VV currents in the TSC evolution equation for G is a good approximation.

4. TSC MODELS OF TORUS CONDUCTING STRUCTURES

Conducting structures internal to the TSC computational grid were represented by a series of passive filamentary wires of specified resistivity. Figure 2 illustrates the filamentary models for the VV, the IC coils, and the inner toroidal field (TF) support structure, all of which are located within the computational grid. Also shown are toroidal current and poloidal flux contours for a typical equilibrium.

Because the thickness and composition of the VV varied poloidally, the VV was modeled as several poloidal segments having resistivities ranging from 1.2×10^{-6} to

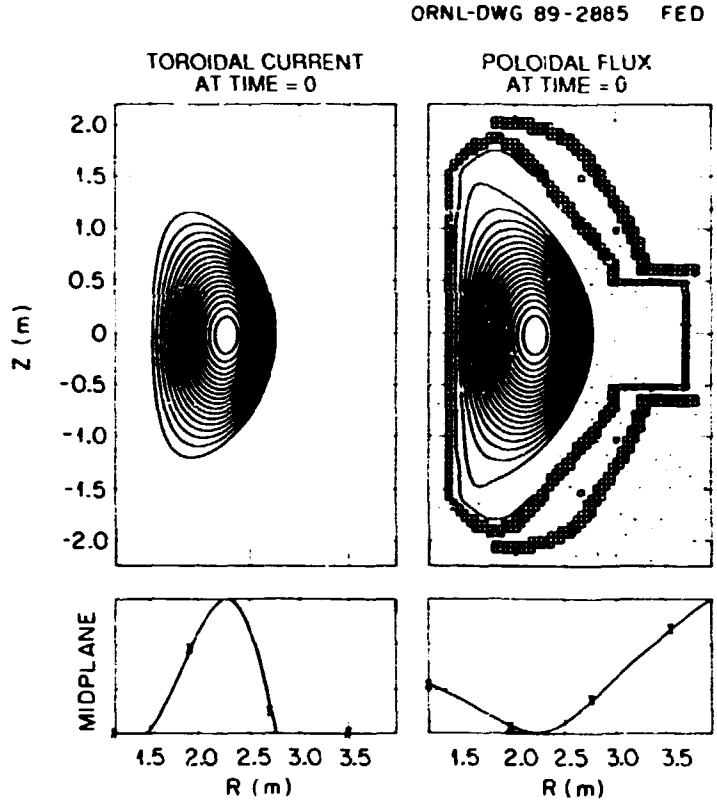

Fig. 2. Toroidal current and poloidal flux contours for a typical equilibrium (I_p = 11 MA, B_t = 10 T, R_0 = 2.102 m, a = 0.645 m, β_{pol} = 0.83, κ_{95} = 1.95, δ_{95} = 0.43, $l_i/2$ = 0.41). Also shown are filamentary models for the VV, IC coils, and inner TF structure, all located within the TSC computational grid.

1.6×10^{-6} Ω·m. For each segment the resistivity was adjusted so that the equivalent TSC resistance was equal to the resistance of the actual geometric shell.

The code SPARK[3] was used to determine the geometry and resistivity of the TSC port so as to give an axisymmetric approximation of the electromagnetic response of the actual ports located at 20° intervals around the torus.

The toroidal resistance of the VV shell was computed from the shell geometry to be 23.9 μΩ. The effective TSC toroidal resistance was obtained by imposing a constant voltage on the TSC grid and allowing the VV current to reach a steady-state value. This procedure yielded a value of 24.5 μΩ, in good agreement with the geometric value. The poloidal VV resistance is 18 μΩ, and the poloidal VV inductance is 0.470 μH.

Two independent copper IC coils ($\rho = 0.27 \times 10^{-8}$ Ω·m) were located at 2.65 ± 1.50 m and 3.00 ± 1.00 m.

The procedure for modeling the inner TF support structure was similar to that for the VV. The material was assumed to be stainless steel 316 with $\rho = 0.55 \times 10^{-6}$ Ω·m, giving a total toroidal resistance of 16 $\mu\Omega$.

Seven poloidal field (PF) coils located outside the TSC computational grid are depicted in Fig. 3. Table 1 contains a typical configuration of PF coil coordinates and initial current values required for the initial plasma equilibrium. Circuit equations in TSC permitted currents to be induced in the PF coils during the disruption simulations, thereby giving a realistic treatment of the inductive coupling of the VV with the PF coils.

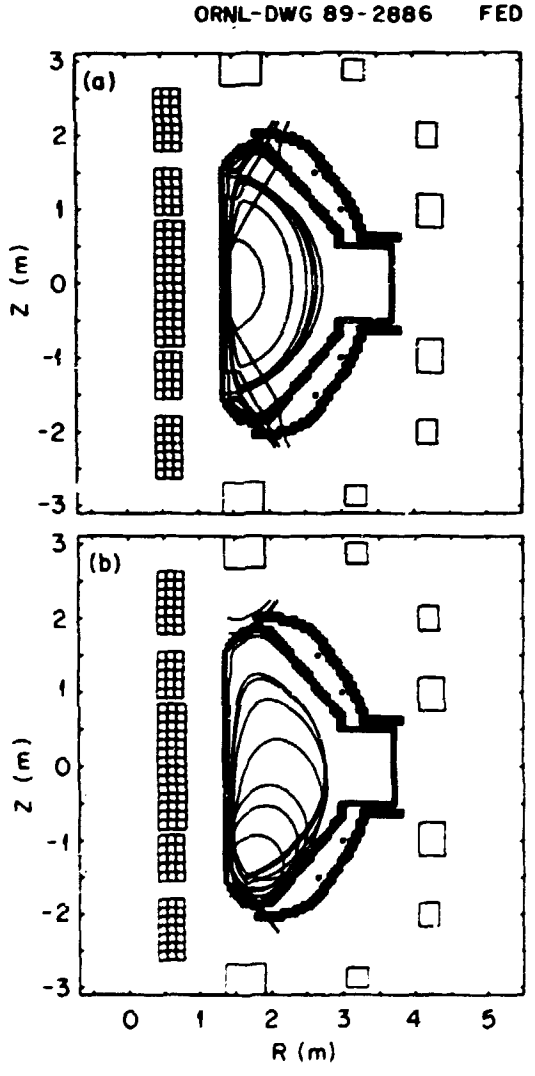

Fig. 3. Plasma boundary evolution during typical (a) radial and (b) vertical disruption scenarios. Representations of the VV, IC coils, inner TF structure, and external PF coils are shown.

Table 1. CIT 2.10-m TSC disruption simulations

(a) Typical initial plasma parameters

R_0 (m)	a (m)	I_p (MA)	B_{tor} (T)	β	β_{pol}	$l_i/2$
2.10	0.646	11.0	10.0	0.049	0.82	0.41

(b) Coil configuration

Coil	$N_R \times N_Z$	R_{center} (m)	Z_{center} (m)	I (MA)
PF1	3 × 7	0.4748, 0.6105, 0.7462	0.060, 0.180, 0.300, 0.420, 0.540, 0.660, 0.780	−0.693
PF2	3 × 5	0.4698, 0.5955, 0.7212	0.983, 1.109, 1.235, 1.361, 1.487	0.420
PF3	3 × 7	0.4698, 0.5955, 0.7212	1.850, 1.970, 2.090 2.210, 2.330, 2.450, 2.570	−0.019
PF4	1 × 1	1.630	2.891	4.993
PF5	1 × 1	3.190	2.870	0.152
PF6	1 × 1	4.187	2.000	−0.823
PF7	1 × 1	4.226	0.976	−5.500
IC1	1 × 1	2.650	1.500	
IC2	1 × 1	3.000	1.000	

5. CIT 2.1-m DISRUPTION SCENARIOS AND VV FORCES

The disruption modeling process can be summarized as follows:

1. Representation of the VV and other conducting structures as resistive loops.
2. Choice of initial conditions: plasma current, beta, plasma shape, vertical displacement, etc.
3. Choice of plasma current decay rate dI_p/dt.
4. Simulation of the disruption with TSC and examination of the evolution of induced currents and J × B forces with the TWIR postprocessor, continuing until the net forces of interest have reached a small fraction of the extreme values.

The preceding process was used repeatedly to study the sensitivity of net VV forces to (dI_p/dt) and to various initial conditions to establish a set of credible disruption scenarios that produced the most severe loads. For these scenarios, the TSC output current and force histories have been made available[6] for use in the structural analysis process.

5.1. EQUILIBRIUM AND INITIAL CONDITIONS

Initial PF coil currents were determined for each set of equilibrium conditions $(R_0, a, \beta_{pol}, \kappa)$ with the equilibrium code[7] of the Oak Ridge National Laboratory's Fusion Engineering Design Center. With these initial PF current values, TSC

quickly converged to an equilibrium that was used as a starting point for radial disruption simulations.

A typical set of initial plasma parameters and an initial PF coil configuration are presented in Table 1. The Troyon beta limit ($3.0I/aB = 4.9\%$) value was used for all disruption scenarios discussed in this report.

For simulation of vertically moving disrupting plasmas, an initial vertical displacement was introduced, and the plasma was then evolved according to the transport equations, with the vertical feedback system disconnected. Evolution was continued until the edge q dropped to 2.1 and the magnetic axis was 45 cm below midplane. At this time, the thermal quench was initiated by enhancement of the plasma thermal conductivity by a factor between 1000 and 20,000, which produced an enhanced plasma resistivity and the subsequent current quench phase. After thermal quench the plasma vertical motion accelerates until the plasma is subject to restriction by a set of limiters near the first-wall and divertor locations. Plasma current, trajectory, and velocity evolution is depicted in Fig. 4, where boxes are plotted at equal time increments, with the area of each box proportional to I_p.

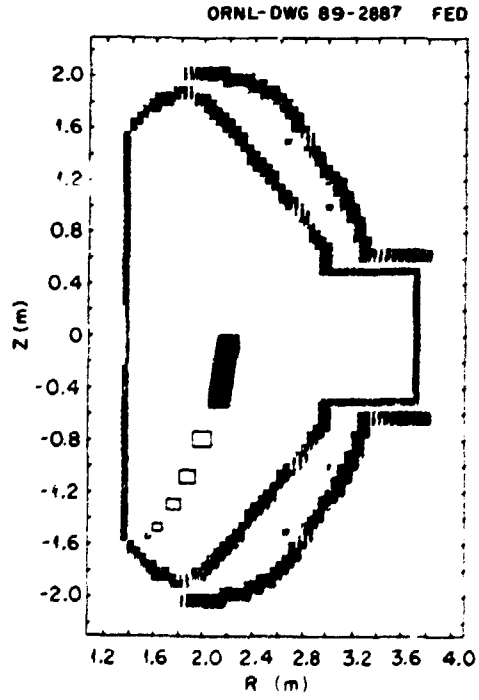

Fig. 4. Plasma current and trajectory evolution for a CIT vertical disruption with $\langle dI_p/dt \rangle = -0.6$ MA/ms. Boxes with area proportional to I_p are plotted at equal time increments.

Motion of the plasma boundary during a disruption is illustrated in Fig. 3, which shows overlays of plasma boundaries for typical radial and vertical disruption examples.

5.2. FORCE DISTRIBUTIONS AND NET FORCE EVOLUTION

Figures 5 and 6 present a time history of force distributions for the CIT 2.1-m VV for a typical vertical disruption. Initial plasma parameters were $I_p = 11$ MA, $\beta = 4.9\%$, $\beta_{pol} = 0.82$, $R_0 = 2.10$ m, and $a = 0.65$ m, and $\kappa_{95} = 1.96$. An initial displacement was introduced, and the plasma was then evolved until the edge q dropped to 2.1 and the magnetic axis was 45 cm below midplane. At this time (170.2 ms), the disruption was initiated by enhancing the thermal conductivity by a factor of 1000 so that $\langle dI_p/dt \rangle = -0.35$ MA/ms. The left, center, and right columns in Figs. 5 and 6 display forces due to toroidal VV currents only, poloidal VV currents only, and both toroidal and poloidal VV currents, respectively. The inner TF support structure is represented by the "backward C" group of filaments. In each frame the cumulative trajectory of the magnetic axis is plotted.

The forces due to poloidal VV currents are clearly comparable in magnitude to forces due to toroidal VV currents during the first 10 ms of the current quench. In addition, the force distribution is highly asymmetric, and large moments exist at several locations.

Figure 7 presents a summary of the net radial VV force F_R, the net vertical VV force F_Z, and contributions to F_R from poloidal and toroidal VV currents as functions of time for a Troyon beta (4.9%) vertical disruption for $\langle dI_p/dt \rangle = -3.4$, -0.6, and -0.35 MA/ms. For these same current decay rates, Fig. 8 displays the plasma current, total toroidal VV current, and the total poloidal VV current as functions of time.

5.3. POLOIDAL VV CURRENT EFFECTS FOR DISRUPTIONS WITH $\beta_{pol} = 0.82$

The relative importance of poloidal VV currents for VV forces clearly depends on the initial value of β_{pol} as well as on $\langle dI_p/dt \rangle$. However, we note here the poloidal VV current effects for a set of disruption simulations, all with initial $\beta_{pol} = 0.82$ and an equilibrium consistent with the baseline CIT 2.1-m design.

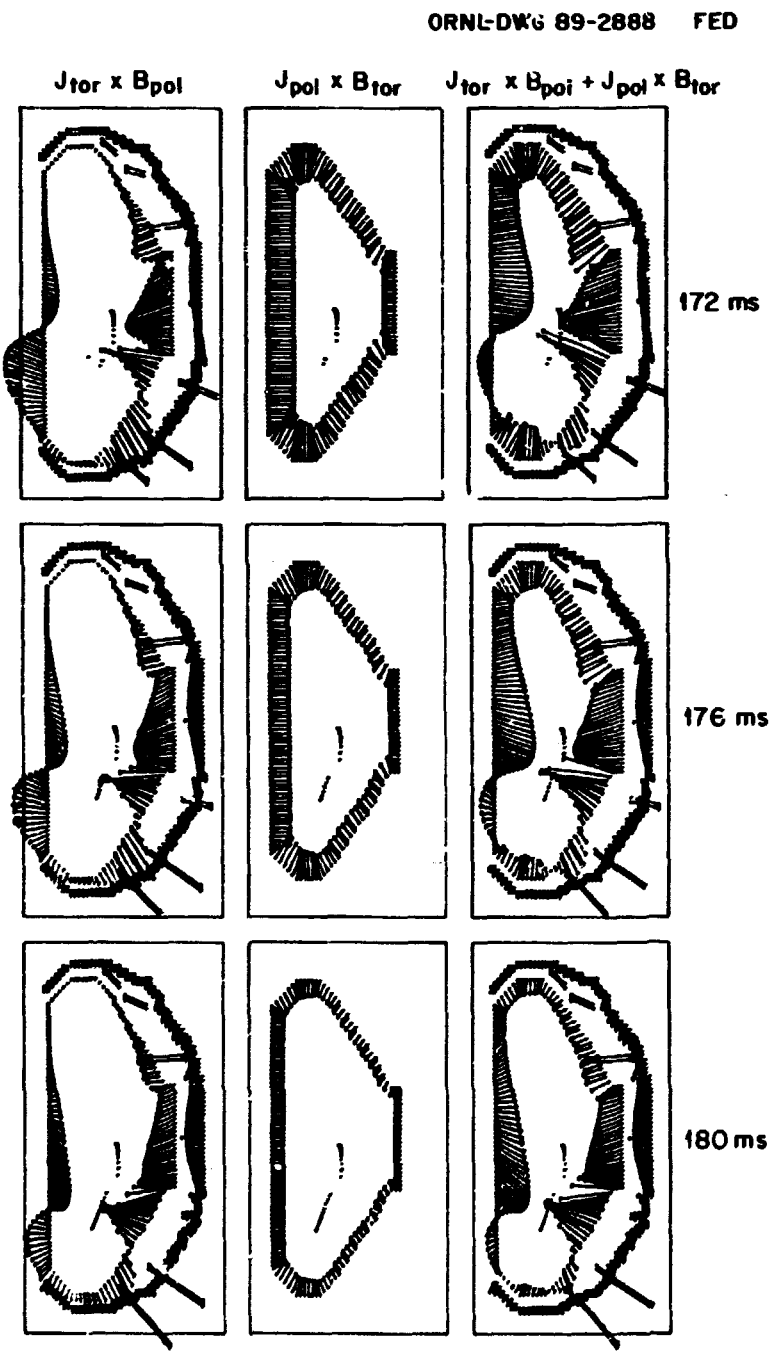

Fig. 5. Time history of force distributions for the CIT 2.1-m VV for a vertical disruption with $\langle dI_p/dt \rangle = -0.35$ MA/ms from 172 to 180 ms. Initial plasma parameters were $I_p = 11$ MA, $\beta = 4.9\%$, $\beta_{pol} = 0.82$, $R_0 = 2.10$ m, $a = 0.65$ m, and $\kappa_{95} = 1.96$. The thermal quench was begun at time 170.2 ms. The left, center, and right columns display forces due to toroidal VV currents only, poloidal VV currents only, and both toroidal and poloidal VV currents, respectively. The inner TF support structure is represented by the "backward C" group of filaments. In each frame the cumulative trajectory of the magnetic axis is plotted.

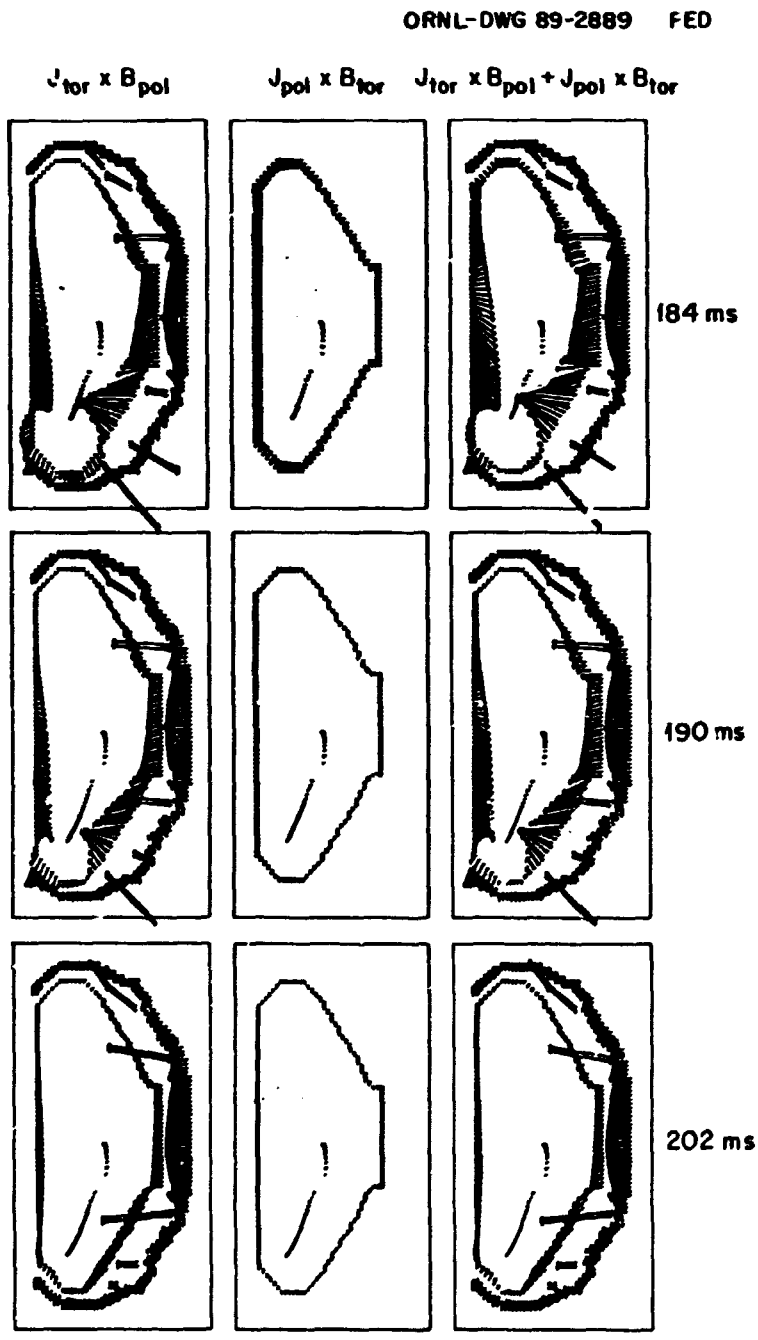

Fig. 6. Time history of force distributions for the CIT 2.1 m VV for a vertical disruption with $\langle dI_p/dt \rangle = -0.35$ MA/ms from 184 to 202 ms. Initial plasma parameters were $I_p = 11$ MA, $\beta = 4.9\%$, $\beta_{pol} = 0.82$, $R_0 = 2.10$ m, $a = 0.65$ m, and $\kappa_{95} = 1.96$. The thermal quench was begun at time 170.2 ms. The left, center, and right columns display forces due to toroidal VV currents only, poloidal VV currents only, and both toroidal and poloidal VV currents, respectively. The inner TF support structure is represented by the "backward C" group of filaments. In each frame the cumulative trajectory of the magnetic axis is plotted.

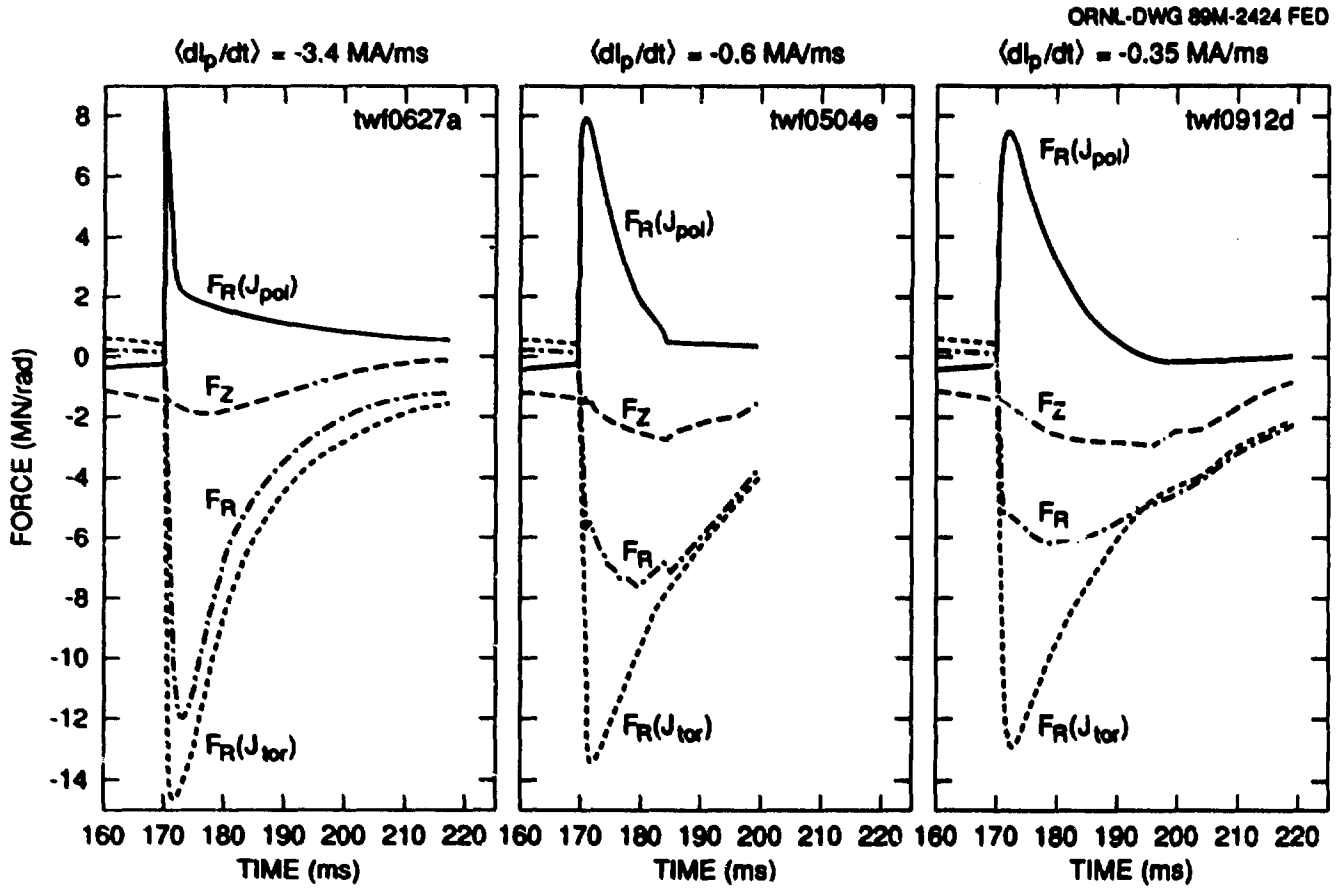

Fig. 7. Net VV forces F_R and F_Z and contributions to F_R from poloidal and toroidal VV currents vs time for vertical disruptions. Initial plasma parameters were $I_p = 11$ MA, $\beta = 4.9\%$, and $\beta_{pol} = 0.82$.

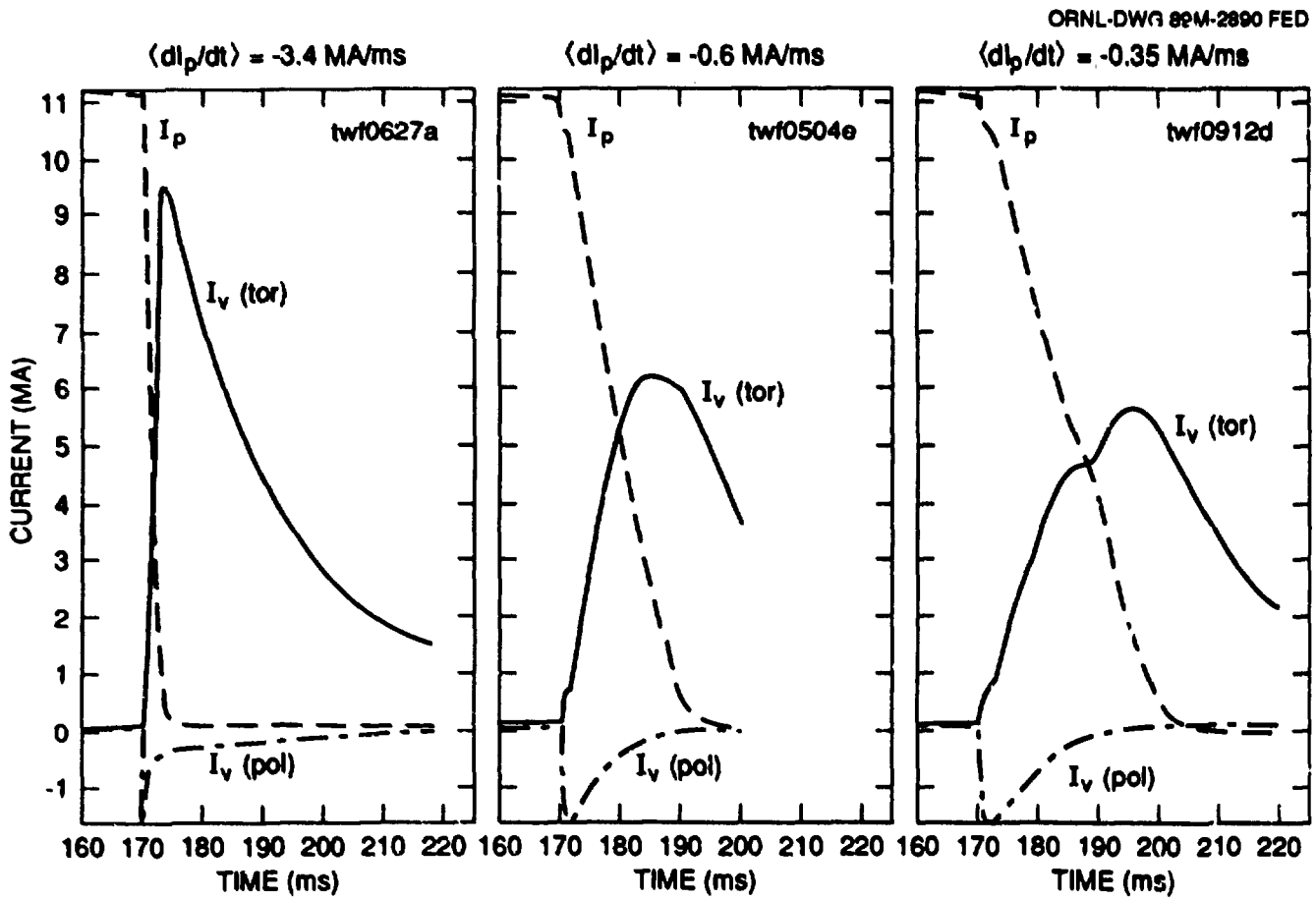

Fig. 8. Plasma current I_p, total toroidal VV current I_V(tor), and total poloidal VV current I_V(pol) vs time for vertical disruptions. Initial plasma parameters were $I_p = 11$ MA, $\beta = 4.9\%$, and $\beta_{pol} = 0.82$.

1. The net vertical force due to poloidal VV currents is zero.
2. Net radial forces due to induced poloidal and toroidal VV currents are opposite in sign.
3. Poloidal VV currents and forces peak soon after the end of the thermal quench.
4. Let F_R(pol) and F_R(tor) be the net radial VV forces due to poloidal and toroidal currents, respectively. Just after the thermal quench, at the time of extreme F_R(pol), we find

$$F_R(\text{pol}) = -0.60 F_R(\text{tor}) \quad .$$

The result [Eq. (5)] is nearly independent of $\langle dI_p/dt \rangle$ since the induced currents at this time are determined almost entirely by geometry.

5. The maximum reduction in magnitude of F_R due to poloidal currents occurs for the slowest current decay rate.
6. The forces due to poloidal VV currents are compressive, yielding a maximum inward pressure of 2.8 MPa for $\langle dI_p/dt \rangle = -3.4$ MA/ms.

Although poloidal VV currents act to mitigate the net inward VV forces due to toroidal VV currents, poloidal VV currents increase the maximum inboard forces by a factor of about two. The present simulations indicate that poloidal VV currents substantially alter the distribution of VV forces and must be taken into account in simulations of major disruptions for tokamak VV design.

5.4. EFFECT OF $\langle dI_p/dt \rangle$ ON VV FORCES

Figure 9, a plot of F_R and F_Z vs $\langle dI_p/dt \rangle$, illustrates both the large ratio of radial to vertical forces and the relatively weak dependence: $F_R \sim |\langle dI_p/dt \rangle|^{0.3}$. The magnitude of F_Z increases from 2 to 3 MN/rad when $|\langle dI_p/dt \rangle|$ decreases from 3.4 to 0.35 MA/ms.

A reduction in decay rate decreases the magnitude of extreme F_R values but increases the magnitude of extreme F_Z values by about 50%, since the current decay proceeds, on average, along a plasma trajectory farther off the midplane than is the case for faster decay rates.

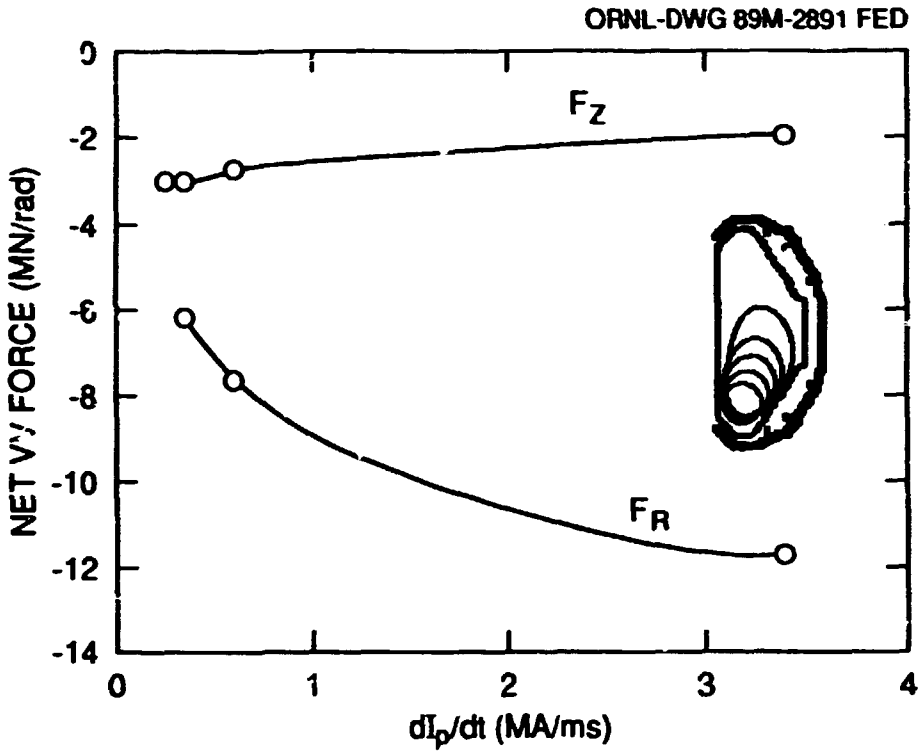

Fig. 9. Extreme net VV forces F_R and F_Z vs $\langle dI_p/dt \rangle$ for vertical disruptions. $F_R = \mathbf{J}_{tor} \times \mathbf{B}_{pol} + \mathbf{J}_{pol} \times \mathbf{B}_{tor}$. Initial plasma parameters were $I_p = 11$ MA, $\beta = 4.9\%$, and $\beta_{pol} = 0.82$.

6. SUMMARY AND CONCLUSIONS

The TSC and the TWIR postprocessor code have been used to develop credible, "highly severe" plasma disruption scenarios for the CIT in order to predict the evolution of forces on CIT conducting structures and to provide results required for detailed structural design analysis. For the set of scenarios discussed here, the extreme values of net radial and vertical VV forces are -12.0 MN/rad and -3.0 MN/rad, respectively, for the CIT 2.1-m, 11-MA design.

Net VV force evolution was found to be altered significantly by two mechanisms not noted previously. The first, due to poloidal VV currents arising from increased plasma paramagnetism during thermal quench, reduces the magnitude of the extreme F_R by 15–50% and modifies the distribution of forces substantially. The second effect is that slower plasma current decay rates give more severe net vertical VV loads because the current decay occurs when the plasma has moved farther from midplane than is the case for faster decay rates.

Both poloidal VV currents and slower current decay rates (0.3–0.6 MA/ms) must be taken into account in simulations of major disruptions for tokamak VV design.

7. FUTURE WORK

An effort is now under way to perform a detailed comparison of TSC and SPARK predictions for currents and forces on passive conducting structures. TSC plasma current distribution output is being used as a SPARK input driver, and closely corresponding models of conducting structures are being used in the two codes.

Future TSC disruption simulations will include a hyperresistivity term in the mean field Ohm's law to reproduce the experimentally observed current rise at the start of the disruption. Also in progress is the addition of the effect of a plasma halo during the disruption which causes force-free currents to flow on the open field lines outside the main plasma and return through the plasma wall. There is a continuing effort to calibrate the TSC model with new experimental disruption data from existing tokamaks.

ACKNOWLEDGMENT

The author acknowledges valuable discussions with W. Reiersen of the Princeton Plasma Physics Laboratory.

REFERENCES

1. S. C. Jardin, N. Pomphrey, and J. Delucia, "Dynamic Modeling of Transport and Positional Control of Tokamaks," *J. Comput. Phys.* **66**, 481 (1986).
2. B. J. Merrill and S. C. Jardin, "DSTAR: A Comprehensive Tokamak Resistive Disruption Model for Vacuum Vessel Components," *Fusion Eng. Des.* **5**, 235 (1987).
3. D. W. Weissenburger and U. R. Christensen, "A Network Mesh Method to Calculate Eddy Currents on Conducting Surfaces," *IEEE Trans. Magn.* **MAG-18**, 422 (1982); D. W. Weissenburger, *SPARK Version 1.1 User Manual*, PPPL-2494, Princeton Plasma Physics Lab., Princeton, N.J., 1988.
4. R. O. Sayer, Y-K. M. Peng, and S. C. Jardin, "Disruption-Induced Forces on a Vacuum Vessel from TSC Poloidal Eddy Currents," *Bull. Am. Phys. Soc.* **33**, 1972 (1988).
5. S. C. Jardin et al., "Modeling of Post-Disruptive Plasma Loss in the Princeton Beta Experiment," *Nucl. Fusion* **27**, 569 (1987).
6. R. O. Sayer, "TSC Disruption-Induced Forces on the CIT 2.10 m Vacuum Vessel," FEDC-L-88-PE-035, Martin Marietta Energy Systems, Inc., Oak Ridge Natl. Lab., Fusion Engineering Design Center, 1988.
7. D. J. Strickler, J. B. Miller, K. E. Rothe, and Y-K. M. Peng, "Equilibrium Modeling of the TFCX Poloidal Field Coil System," ORNL/FEDC-83/10, Union Carbide Corp. Nuclear Div., Oak Ridge Natl. Lab., April 1984.